Nuclear Science and Techniques (2023) 34:53
https://doi.org/10.1007/s41365-023-01211-5

TLD calibration and absorbed dose measurement in a radiation-induced liver injury model under a linear accelerator

Hui-Hui Xiao[1] · Ling-Ling Liu[3,4] · Wen-Yi Li[5] · Bing-Bing Li[2] · Xiang-Li Cui[2,3] · Jie Li[3] · Tao-Sheng Li[5] · Zong-Tao Hu[1,2]

Received: 14 November 2022 / Revised: 20 February 2023 / Accepted: 27 February 2023 / Published online: 18 April 2023

Abstract

The application of a thermoluminescent detector (TLD) for dose detection at the liver irradiation site in mice under linear accelerator precision radiotherapy and the use of a single high dose to irradiate the mouse liver to construct a biological model of a radiation-induced liver injury (RILD) in mice were to determine the feasibility of constructing a precision radiotherapy model in small animals under a linear accelerator. A 360° arc volumetric rotational intensity-modulated radiotherapy (VMAT) plan with a prescribed dose of 2 Gy was developed for the planned target volume (PTV) at the location of the TLD within solid water to compare the difference between the measured dose of TLD and the assessed parameters in the TPS system. The TLD was implanted in the livers of mice, and VMAT was planned based on TLD to compare the measured and prescribed doses. C57BL/6 J mice were randomly divided into control and 25-Gy radiation groups and were examined daily for changes in body weight. They were euthanized at 3 and 10 weeks after radiation, and the levels of liver serum enzymes such as alanine aminotransferase (ALT), aspartate aminotransferase (AST), and alkaline phosphatase (ALP) were measured to observe any pathological histological changes in the irradiated areas of the mouse liver. The measured values of solid underwater TLD were within ± 3% of the D_{mean} value of the evaluation parameter in the TPS system. The mice in the 25-Gy radiation group demonstrated pathological signs of radiation-induced liver injury at the site of liver irradiation. The deviation in the measured and prescribed doses of TLD in the mouse liver ranged from − 1.5 to 6%; construction of an accurate model of RILD using the VMAT technique under a linear accelerator is feasible.

Keywords Thermoluminescent detector · Radiation-induced liver injury · Linear accelerator · Volumetric rotational intensity-modulated radiotherapy

1 Introduction

Recently, based on the rapid development of volumetric rotational intensity-modulated radiotherapy (VMAT), most patients with inoperable or locally advanced liver cancer have achieved good results with precision radiotherapy [1]. VMAT allows for the rotational irradiation of the target area at any angle within any 360° single- or multi-arc setting, which is more flexible and precise than using conventional treatment modalities. It can improve the conformality and homogeneity of the target area of the liver, reduce the high-dose irradiation to the surrounding normal liver tissues, and efficiently protect normal liver tissues [2]. However, the liver is highly radiosensitive, and radiation-involved normal liver tissues are significantly susceptible to radiological liver injury. Once RILD occurs, it continues to develop over time, resulting in advanced radiation liver fibrosis damage and

This work was supported by the Natural Science Foundation of Anhui Province (No. 2208085MA13), Wu Je Ping Medical Foundation (No. 320.6750.2020-10-40), and the Key Research and Development Program of Anhui Province (No. 202004J07020052).

✉ Zong-Tao Hu
huxuyan@163.com

1 School of Basic Medical Sciences, Anhui Medical University, Hefei 230000, China

2 Hefei Cancer Hospital, Chinese Academy of Sciences, Hefei 230000, China

3 Institute of Health and Medical Technology, Hefei Institute of Materials Science, Chinese Academy of Sciences, Hefei 230000, China

4 University of Science and Technology of China, Hefei 230000, China

5 Hefei Institute of Materials Science, Chinese Academy of Sciences, Hefei 230000, China

liver failure in most patients, and eventually death. The physiological pathogenesis of RILD remains unclear, and there is a lack of effective clinical treatments. Whole-genome sequencing has been completed for C57BL/6 J mice, confirming that 99% of its genes are homologous to the human genome. This is advantageous for the single-cell sequencing of radiation-induced liver injury and subsequent molecular pathogenesis studies; therefore, it is necessary to establish a suitable mouse model for RILD mechanism studies and exploring intervention strategies [3, 4]. Linear accelerators are commonly used medical devices in clinical practice, and the MV radiotherapy system has been sufficiently validated. The Monte Carlo algorithm in the TPS system can simulate particle collision trajectories and the energy distribution in a three-dimensional space, which presents a significantly high computational accuracy and can accurately calculate the dose delivered to the equivalent tissue material. Knowing that the values calculated by the TPS system are correct, the accurate delivery of the radiation dose to the intended area is the main issue [5–7]. Traditional 3D conformal radiotherapy techniques and general radiotherapy are unable to control the amount of radiation received to the organ at risk. In VMAT, the frame is continuously rotated to continuously change the dose rate, frame position, and multi-leaf collimator blade position for adjusting the beam intensity in the direction of the different irradiation fields, which provides good control of the amount of radiation to the organ at risk while satisfying the dose to the target area. Owing to the small size of mice, with an average liver volume of only (1.325 ± 0.029) g, their tendency to move between the computed tomography (CT) simulator and the linear accelerator, the close proximity of the mouse intestine to the liver, and their high sensitivity to radiation, it is challenging to determine the deviation in the position of liver irradiation and the measured dose during the construction of the biological model. Moreover, mice are vulnerable to radiation enteritis and death within a short period, which eventually leads to failure of the biomimetic model of RILD. Therefore, it is worthwhile to examine the deviations in the actual absorbed dose and exposure location in mice liver [8–10].

Various instruments are used in radiation dosimetry for radiation detection and measurements. Finger-type ionization chambers, 2D ionization chamber matrices, EBT3 films, and TLDs are the main radiation detection instruments used for the dose verification of treatment plans using linear accelerators. Clinical dose calibration is generally performed with ionization chamber detectors, where finger-type ionization chambers are used for point dose verification and two-dimensional ionization chamber matrices are used to verify the dose distribution of radiotherapy plans, both of which obtain absolute measurements but demonstrate a limited advantage in small irradiation fields, radiation fields, and in vivo measurements. The EBT3 film has a high spatial resolution and is capable of measuring the dose in a 2D plane to obtain a detailed dose distribution map, but is not suitable for in vivo dose measurements [11]. In conclusion, all the aforementioned measurement instruments obtain the radiation dose in a two-dimensional plane and cannot be applied in dimensional space, demonstrating a limited advantage for dosimetry in VMAT techniques. In addition, TLD and optically stimulated luminescent dosimeter (OSLD) are physically similar; Alvarez et al. demonstrated that only a slight difference was observed between the TLD and OSLD procedures in terms of accuracy measurements [12]. TLD dosimetry possesses properties such as dispersion, precision, detection threshold, measurement range, dose–response rate, spatial resolution, dose-rate response independence, energy independence, and tissue equivalence. Their material versatility and different physical forms allow them to measure different radiation qualities over a wide range of absorbed doses, and they are also advantageous in dose distribution measurements caused by techniques such as 3D conformal, intensity-modulated radiotherapy, and computed tomography (CT) [13]. The accuracy of dosimetry in preclinical radiobiology experiments has been a topic of concern, and the mouse liver model involves small-radiation-field dosimetry, for which dosimetry is significantly challenging. Owing to the energy dependence of TLD, the typical area of interest includes radiobiological experiments using kV X-rays without a validated and reliable treatment planning system. Kuess et al. [14] suggested that TLD can be used for in vivo measurements in mice using commercially lower X-ray equipment. Karagounis et al. implanted TLD into the chest and lungs of mice immobilized on PMMA devices and provided a three-dimensional conformal plan, proposing that TLD can validate the dosimetry of radiation treatment plans for radiation beams and scattered rays. However, the absorbed dose of radiation in preclinical mice was not defined [15]. The objective of this study is to investigate the use of TLD in precision radiotherapy using a linear accelerator, with a focus on determining the actual absorbed dose at the location of radiation in the livers of mice. Furthermore, the study aims to assess the feasibility of creating a precise model of radiation-induced liver disease (RILD) in mice using the VMAT technique under a linear accelerator.

2 Materials and methods

2.1 Experimental materials

The TLDs used in this study were LiF: Mg, Cu, P TLDs manufactured by Beijing Guang Yi Ruitong Company, model GR-200 A. They were available in cylindrical or square shapes and three different sizes, including a 4.5-mm piece measuring 4.5 mm × 4.5 mm × 0.8 mm, a 3.6-mm piece

measuring 3.6 mm × 3.6 mm × 0.4 mm, and a 1-mm piece measuring 1 mm × 1 mm × 1 mm. All TLD sizes had a dispersion of ± 1%. The equipment used in this study included an annealing furnace and TLD readout system (RGD-3E/D, Beijing Seasuncc Technology Co., Ltd.), a FARMER finger-shaped ionization chamber measuring 0.6 cm^2, an ionization chamber dosimeter (PTW-UNIDOSE), a linear accelerator (infinity, Elekta), a CT analog positioner (Brilliance, Philips), and a Radiotherapy Planning System (MONACO 5.11.03). Additionally, tissue embedding kits and adhesive slides (Jiangsu Shitai Laboratory Equipment Co., Ltd.) were used, as well as an automatic tissue dehydrator, a tissue embedding machine, a pathological tissue bleaching and drying machine, and a paraffin sectioning machine (all from Leica, Germany).

2.2 Animals and feeding methods

Twenty-five C57BL/6 J male mice (6–8 weeks old) were purchased from GemPharmatech Co., Ltd., all of which were housed in a pathogen-specific environment (SPF class) with free access to water and standard feeding in a 12-h day/night environment. The Medical Ethics Committee of Hefei Cancer Hospital, Chinese Academy of Sciences approved all experimental procedures, including humane measures to reduce the suffering of the mice. To ensure minimal discomfort, five mice were euthanized with an overdose of tribromoethanol anesthesia before the start of the TLD assay in the liver.

2.3 TLD detector principle and usage

TLDs possess a crystal structure in which irradiation by radiation results in an ionization excitation effect that causes some electrons to become excited into a sub-stable state. The location of the electron deficiency forms a lattice defect, known as the hole. These holes have capability to trap electrons, and when the crystal is heated, the thermal motion of the trapped electrons reaches the conduction band, and the electrons in the conduction band are deexcited into the ground state, and the deexcitation process emits light. A TLD readout system heats the TLD that receives the irradiation and measures the TLD output using a photomultiplier tube to determine the radiation dose value.

The TLD is measured with a TLD readout system, and the measurement heating procedure is divided into two stages of programmed heating; the first stage is preheating at 135 °C for 8 s, and the second stage is heating at a constant temperature of 240 °C for 12 s. After the measurement, the TLD was placed in an aluminum tray at a constant temperature of 240 ± 2 °C, annealed for 10 min, rapidly cooled to room temperature, and placed into a lead chamber [16].

2.4 TLD calibration

The ionization chamber dosimeter was situated 5 cm below equivalent solid water. The irradiation field was 10 cm × 10 cm in size, with the radiation source to skin distance (SSD) set at 100 cm. The percentage depth dose ratio (PDD) was determined to be 86.6% at 5 cm above the central axis of the beam. A 6 MV X-ray beam was used to emit 100 MU, and the ionization chamber dosimeter measured the value to verify that the final dose output was calibrated to 1 cGy = 1 MU [17, 18].

The same batch of the TLD was irradiated with a linear accelerator at 5 MU under 1.5 cm of solid water (SSD = 100 cm, irradiation field size of 10 cm × 10 cm), and the TLD count values were recorded. Each TLD had a unique coded number, and the background count was deducted to find the reading value E and the standard deviation S_E of each TLD. The TLD is calculated as $S_E/\overline{E}$, which is repeated three times after annealing to calculate the total mean $\overline{E}$ of all the dose slices irradiated three times and the corresponding standard deviation S_E; the repeatability is calculated as: $S_E/\overline{E}$. Because the dispersion differences provided by the commercial TLDs were screened under cobalt source irradiation, which is different from the linear accelerator used in the experiments, the batch of TLDs underwent another screening process under the linear accelerator to ensure consistency. TLDs with dispersion and reproducibility errors of less than 1.5% were selected for this experiment [19].

With 6 MV X-rays at a dose rate of 600 cGy/min, SSD = 100 cm, an irradiation field of 10 cm × 10 cm, PDD = 100% at 1.5 cm above the beam center axis, the screened and annealed TLD was divided into seven groups with four TLDs in each group and placed at a 1.5 cm depth of equivalent solid water. After emitting beams of 5, 30, 50, 70, 100, 150, 200, and 300 MU, the real value of each TLD was recorded and the mean value M of each group of the measured data was calculated by subtracting the background count to obtain the scale factor of this batch of TLDs [20]. The TLD scale factor N is the quotient obtained by dividing the number of beam monitor units H of the linear accelerator by the mean reading value M of the TLDs, namely $N = H/M$

2.5 TLD detection under precision radiotherapy

2.5.1 TLD detection under solid water

The dose that can be received under ideal conditions is unknown for the precision irradiation of a TLD under a linear accelerator. To explore the dose that TLD can receive

under precision radiotherapy, the difference between the measured and prescribed doses of TLD was assessed to determine the correlation with the target area assessment parameters of D_{max}, $D_{mean,}$ and D_{min} in the planning system. One graduated 4.5-mm piece fixed in solid water with a lower layer of 6 cm and covered with 1.5 cm was positioned and scanned using a CT simulator. The TLD had a density close to the bone cortex (approximately 2.5 g/cm^3) and was developed in the CT images; the TLD was outlined and named PTV. Under a linear accelerator, a VMAT plan was designed with a prescription dose of 2 Gy and a 360° arc. The maximum dose was planned to be within 110% of the prescribed dose, as evaluated according to the requirement of a 100% isodose curve wrapped around 100% of the PTV volume. The plan was then irradiated; the radiotherapy dose is schematically shown in Fig. 1 Considering that CT scans can have a dose effect on TLDs, four additional TLDs were CT scanned under the same conditions at the same location. The CT scan dose was obtained by reading out the measured values after the CT scans and calculating their average value. The background D_{CT} had a measured value of 3.31 cGy. The measured value of the solid water TLD (D_S) is the dose of the background D_{CT} removed from the reading value of the solid water TLD.

2.5.2 TLD detection under the mouse liver

The mice were fixed in the supine position on a carbon fiber plate, and plastic sheets were attached to both sides of the plate to place the lead dots and mark the localization line. After the mice were anesthetized to death by overdosing with chloral hydrate, the surgeon inserted a sealed 4.5-mm piece into the mouse liver and sutured it closed. The CT was positioned and scanned at a minimum thickness layer of 1 mm. The physicist outlined the target area on the CT image using the TLD as the PTV and provided a VMAT plan with a prescription dose of 2 Gy and 360° arc, where the calculation grid was 1 mm in size, the subfield width was 0.5 mm, the calculation uncertainty was 1%, the maximum dose was required to be within 110% of the prescription dose, and the requirement for a 100% isodose curve wrapped around 100% of the PTV volume was followed; the radiotherapy dose is schematically shown in Fig. 2. After irradiation, the surgeon removed the TLD and placed a new TLD in the same location in the mouse liver and then repeated the procedure. To ensure reproducibility, five mice were used in this experiment, and the same procedure was repeated three times for each mouse. As indicated above, the mouse liver D_{CT} value was 3.51 cGy. The measured value of the mouse liver TLD

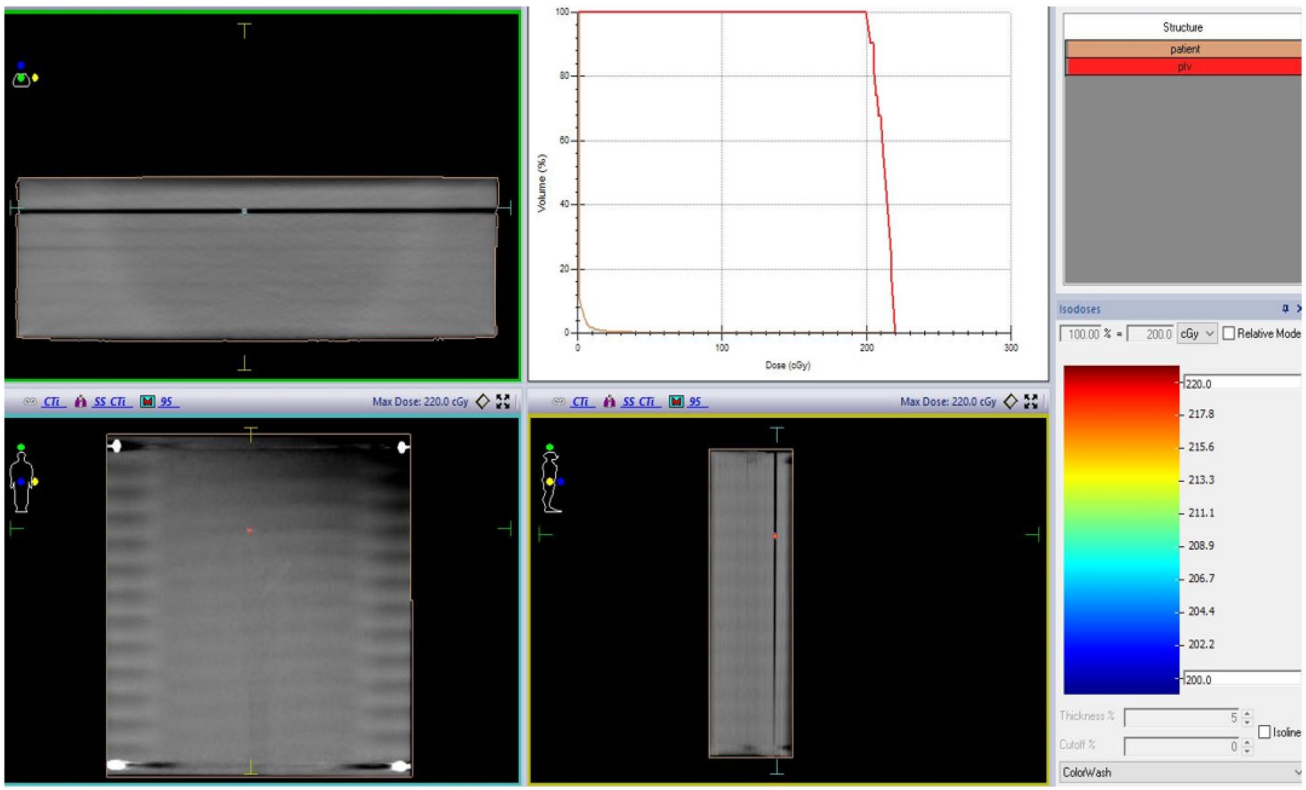

Fig. 1 (Color online) Schematic of the dose of solid in-water TLD radiotherapy (4.5 mm piece) Schematic cross-sectional, sagittal, and coronal views of solid water and dose-volume histograms (DVH plots), where the TLD is the ptv and the solid water surface is the patient

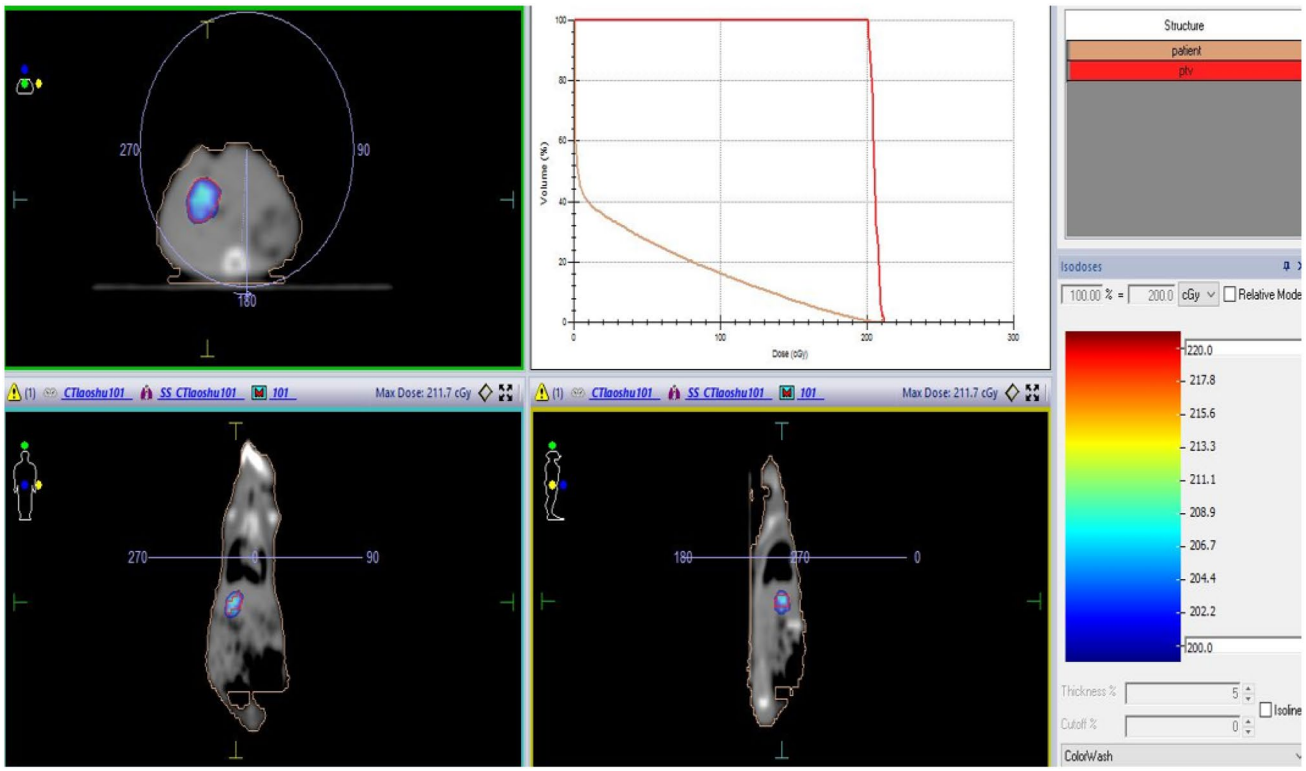

Fig. 2 (Color online) Schematic of the TLD radiotherapy dose in the mouse liver (4.5 mm piece) Cross-sectional, sagittal, and coronal schematics and dose-volume histograms (DVH plots) of mice, where the TLD is the PTV and the mouse skin indicates the patient

(D_L) is the dose of the mouse liver (D_{CT}) removed from the reading value of the mouse liver TLD.

2.6 Radiation-induced liver injury pathological examination

Twenty-five mice were randomly divided into the two following groups, with ten mice in each group: control and 25-Gy radiation-treated. The control group was treated in the same manner as the radiation group, except that no radiation was administered. The mice in the 25-Gy radiation group were anesthetized, immobilized, and positioned on the CT scans. The physician outlined a target area of 0.4 cm in diameter and 0.5 cm in height in the upper right lobe of the liver, the physicist designed a VMAT plan with a prescribed dose of 25 Gy and a 360° arc, the physician assessed it according to the requirement of a 100% isodose curve wrapped around 95% of the PTV volume, and the radiographer positioned the laser light according to the positioning line and delivered the irradiation. Following irradiation, changes in the body weight were recorded daily, and the diet and activity of the mice were observed. Serum was collected from the 25-Gy irradiated mice by orbital blood sampling, and changes in the serum liver enzymes of ALT, AST, and ALP were measured. This study was conducted to determine whether the irradiated mouse liver produced pathological symptoms of radioactive liver injury for investigating the feasibility of constructing a precise radiotherapy model for RILD in mice using a linear accelerator and to further verify the accuracy of the irradiation site in physical experiments.

3 Results

3.1 TLD calibration results

The dispersion and reproducibility distributions of the TLDs are shown in Fig. 3a. Only 50 TLDs are listed in the figure, where the 1–10, 11–20, and 21–50 TLD numbers are for the 1, 3.6, and 4.5 mm pieces, respectively. As shown in the graphs, the dispersion and repeatability values for the 1, 3.6, and 4.5 mm pieces ranged from 2.19 to 2.29, 16.07 to 17.04, and 40.12 to 41.37, respectively. The linear accelerator irradiated 5 MU, and the standard error of the dispersion and repeatability values measured for all three sizes of the TLDs were < 1.5%, demonstrating that the difference in dispersion between the three sizes of the TLDs under the linear accelerator can be as high as 1.5% with good reproducibility after screening. The scaling curves of the TLDs (Fig. 3b) were found to have a coefficient of determination (R^2) equal to 1

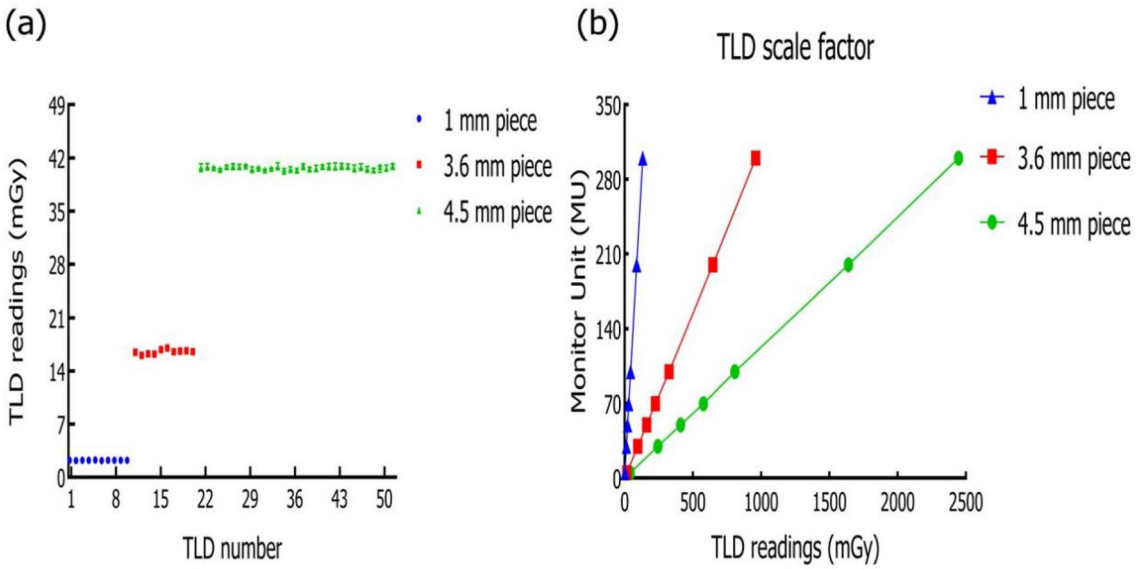

Fig. 3 (Color online) TLD calibration results under the linear accelerators. **a** TLD repeatability and dispersion readings (5 MU); **b** TLD scale factor (1 mm piece linear equation: $y = 2.2708x$, $R^2 = 1$; 3.6 mm piece linear equation: $y = 0.3111x$, $R^2 = 1$; 4.5 mm piece linear equation: $y = 0.1225x$, $R^2 = 1$)

for all three sizes of the TLDs under a linear accelerator with a 6-MV photon beam, demonstrating a linear dose–response ranging from 5 to 300 MU and indicating that the carefully calibrated TLDs can be used for clinical radiotherapy dosimetry with linear accelerators.

3.2 TLD results under precision radiotherapy

The results measured for the TLD in solid water demonstrated that the measured values of the TLD in solid water (D_S) were both up to and above the prescribed dose, with the values varying within $\pm 3\%$ of the D_{mean} parameter assessed in the TPS system (Fig. 4a, b), where S_{max}, S_{mean}, and S_{min} indicate the differences between D_S and the D_{max}, D_{mean}, and D_{min} parameters assessed in the TPS system. The absolute readings of the TLD measured in the liver are shown in Fig. 4c, and the differences between their measured values and the TPS system assessment parameters are shown in Fig. 4d, where L_{pd} is the difference between the measured value of the TLD in the mouse liver (D_L) and the prescribed dose, and L_{mean} is the difference between D_L and D_{mean} of the TPS system. Figure 4d demonstrates that the deviation between the measured dose of the liver TLD and D_{mean} value in the TPS system ranged between -0.6 and -9%, with an overall decreasing trend. The maximum deviation of the measured dose of the TLD in the mouse liver from the prescribed dose is approximately 6%, with slight variability in the irradiation location. Therefore, it can be concluded that a precise radiotherapy model for RILD mice can be constructed under a linear accelerator.

3.3 Pathological results of radiation-induced liver injury

As shown in Fig. 5a, after 10 weeks of radiation at the prescribed dose of 25 Gy, the body weight of the mice in the radiation group gradually decreased compared to that of the control group, and slowly increased until approximately 15 days after radiation. The changes in the serum liver function indicators of the mice are shown in Fig. 5b. Compared to the control group, the levels of ALT and AST in mice increased after 3 and 10 weeks of radiation, and the levels of ALT and AST in mice demonstrated a significant increase after 10 weeks of radiation. In addition, compared to the control mice, ALP levels decreased after 3 weeks of radiation and increased after 10 weeks of radiation. Meanwhile, the results of the pathological sections (Fig. 5c, d) in the control mice demonstrated that normal hepatocytes were arranged in a radiolucent pattern around the central vein, and the liver lobules were clearly outlined. After 3 weeks of radiation, the lobules of the liver in the 25-Gy radiation group were clear structured, with a small amount of lymphocyte infiltration in the confluence area and around the central vein, normal liver plate structure, and turbid swelling and degeneration of hepatocytes. After 10 weeks of radiation, the liver lobules of the 25-Gy radiation group were disorganized, with inflammatory cells infiltrating the confluent area, and the hepatocytes were cloudy and swollen, dotted with degeneration and necrosis. The results demonstrated that mice in the 25-Gy radiation group showed signs of radiation-induced liver damage in the right upper lobe of the liver, which

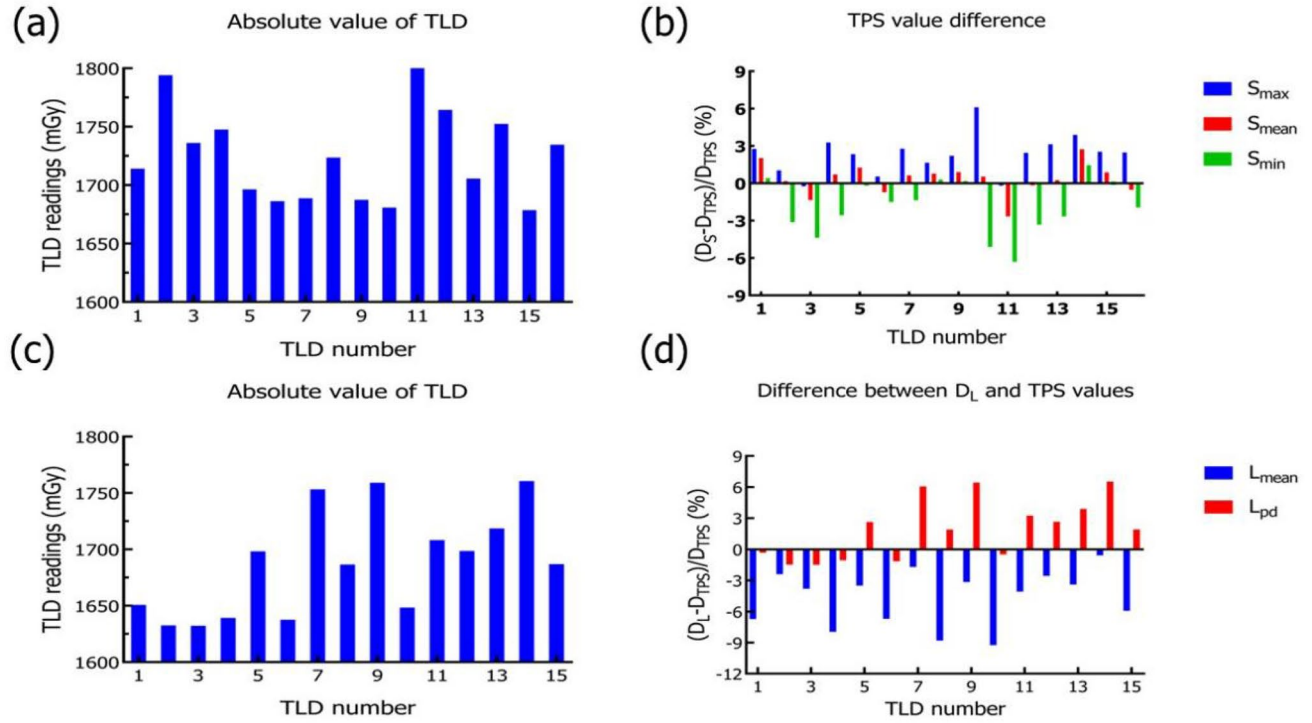

Fig. 4 (Color online) TLD results under precision radiotherapy. **a** Absolute readings of TLD under solid water. **b** Difference between D_S under solid water and each value of TPS. **c** Absolute readings of TLD in the liver. **d** Difference between the intrahepatic D_L and TPS system assessment parameters

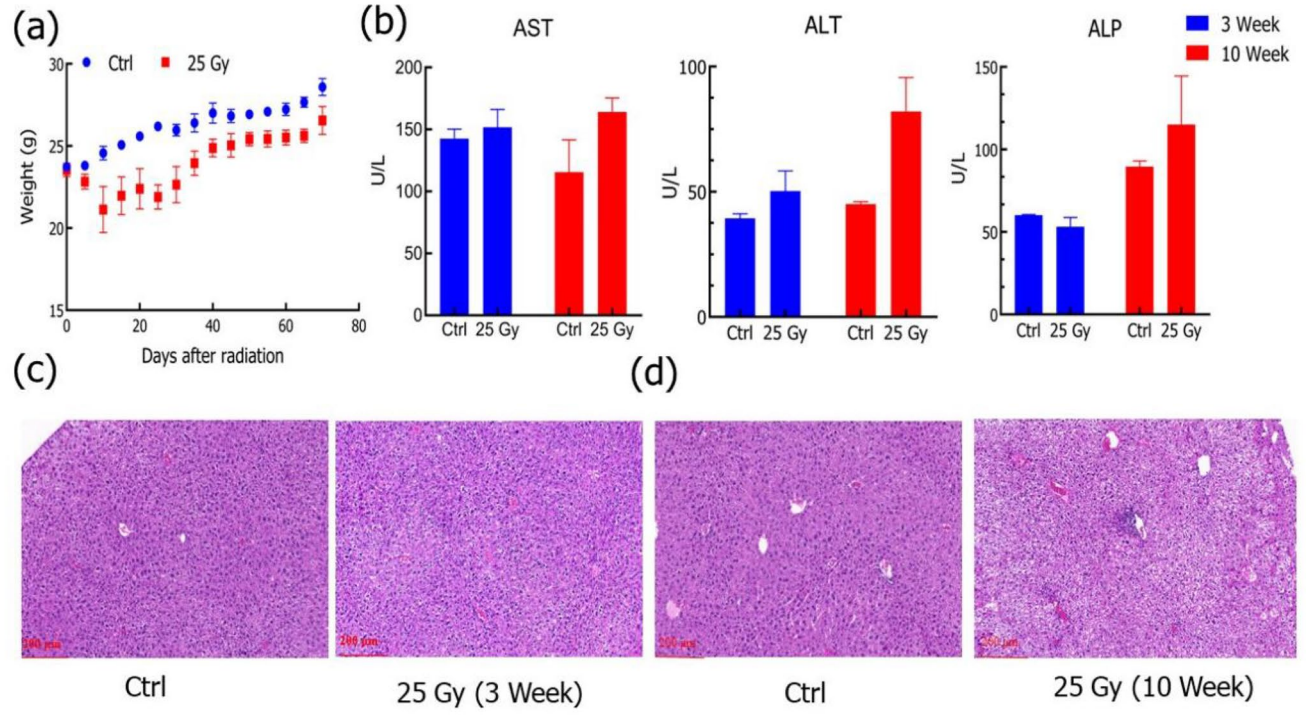

Fig. 5 (Color online) Radiation-induced liver injury of mice in the 25-Gy radiation group. **a** Changes in the body weight of mice (10 weeks). **b** Changes in the serum liver enzymes of ALT, AST, and ALP. **c** Results of the pathological histology of mice liver after 3 weeks of radiation (representative pictures; bar: 200 μm). **d** Results of the pathological histology of mice liver after 10 weeks of radiation (representative pictures; bar: 200 μm)

progressed with time, indicating the potential to develop a precise radiotherapy model for small animals under a linear accelerator.

4 Discussion

TLDs are widely used in the membrane, in vivo measurements, and dosimetric reviews under linear accelerators owing to their small size, high sensitivity, good stability, energy response, and tissue equivalence, as well as convenience for in vivo and ex vivo measurements [21]. Chen et al. obtained equivalent doses for organs or tissues of patients with nasopharyngeal carcinoma under the VMAT program and normal doses by inserting a TLD into human molds [22]. Acun-Bucht et al. found that the TLD readings were consistent with the TPS calculations with a 3% deviation on the central axis in their dosimetric validation of the intensity-modulated radiotherapy (IMRT) scheme, providing a good accuracy for absolute dosimetry [23]. Lai et al. evaluated the therapeutic dose at the nasopharyngeal air-tissue interface using an anthropomorphic model and found that the difference between the calculated TPS dose and measured TLD at the air-tissue interface under a 2 cm × 2 cm field of view was −4.9% [24]. The aforementioned study compared the difference between the TPS dose and TLD measurements under regular radiation fields, that is, the difference in the dose between the TPS system and a point of TLD measured under general radiation conditions, indicating that the TLD has a good measurement accuracy under a linear accelerator. The measurement of TLDs as a relative measurement method presents inherent dispersion errors; this experiment screened for TLDs within the 2% standard deviation of dispersion recommended by Das et al. The actual radiation received by the TLD measured underwater correlated with the evaluation parameters of the target area of the TPS system; a 4.5-mm piece with a similar size to the target area of mice was used in the biological model. The maximum deviation from the prescribed dose was approximately 6% [25]. Liquitab et al. concluded that TLDs can be used for in-patient dosimetry in small- to medium-sized 6-MV photon fields; however, the material in the TLD structure may cause perturbations in the radiation dose in the target volume, and the presence of the dosimeter may alter the local level of the lateral charged particle equilibrium (CPE), producing dose perturbations that affect the radiation dose [26]. The mouse body was only approximately 2 cm thick, the target area of the mouse liver was close to the skin, and backscattered radiation affected the surface dose. Palmer et al. applied TLD for in vivo dosimetry in clinical KV treatment and found that the prescribed dose deviated from the measured dose by −9% in certain cases and that the cavity, bone, and backscatter affected the therapeutic dose [27, 28]. The International Atomic Energy Commission Report 30 defines the biological effect dose (BED) as a measure of the degree of radiological response of an organism. The physical dose (prescribed dose) is not identical to the BED, and the same prescribed dose has different biological effects on the same tissue owing to varying splitting methods or different dose rates. According to the classical radiobiological theory, the dose rate effect in low linear energy transfer (LET) radiotherapy is the primary determinant of the range of biological effects produced by a particular dose. Photons present low LET radiation and the therapeutic dose rate of linear accelerators is relatively constant. Considering radiobiological conclusions, a 10% difference in the therapeutic dose causes a significant difference in the therapeutic gain coefficient; therefore, we believe that the range of the measured differences in the TLD in the liver is acceptable in the construction process of the biological model. The deviations in the irradiation site are not significant, and there is no significant offset in the radiation dose at the irradiation location to ensure an accurate pose. Therefore, a small animal precision radiotherapy model can be constructed under a linear accelerator, and the radiation dose to the mouse liver can be assessed according to the prescribed dose in the TPS system [29, 30].

The study of molecular pathogenesis and protective strategies of RILD is a popular topic in radiation therapy for liver cancer, and the construction of RILD animal models is critical for exploring the pathophysiological mechanisms of RILD. Professor Zeng Zhao Chong found elevated AST and ALT serum levels in mice during the modeling of RILD, as well as fatty degeneration and inflammatory cell infiltration under light microscopy, which is the gold standard for the diagnosis of RILD [31]. Biological data demonstrated that ALT and AST levels increased in the 25-Gy irradiated mice after 3 and 10 weeks of irradiation, and the changes in their levels significantly increased over time. Inflammatory cell infiltration was observed in the irradiated livers of the mice in the radiation group under light microscopy, and the area of liver damage was greater in mice irradiated for 10 weeks compared to 3 weeks of radiation, and its severity also increased over time. The 25-Gy radiation group demonstrated signs of radiation-induced liver injury, such as elevated serum ALT levels, inflammatory cell infiltration, and hepatocyte necrosis. During the observation of the mice after radiation, it was observed that all mice survived for 10 weeks after radiation, indicating that they did not die because of radiation-induced enteritis. This result demonstrates the advantage of the VMAT technique in a linear accelerator and provides a reference value of the radiation dose for the construction of an accurate model of RILD in a single mouse irradiated under a linear accelerator. During the process of the biological model construction, it is appropriate to use a

carbon fiber plate as fixed-body position material for mice. Carbon fiber plates can improve the X-ray penetration ability and reduce the scattered dose to a significant extent [32]. Owing to the small size of the mouse liver, the use of small lead points is appropriate for CT localization. Large lead points increase the positional error, and large metallic artifacts exist in the CT images, which have a greater impact on the dose calculation. Moreover, it was noted that the radiotherapy procedure for a single mouse could take up to an hour, which encompasses several steps such as anesthesia and immobilization of the mouse, CT simulation positioning, outlining of the target area, planning, and linear accelerator irradiation. This process involves the expertise of multiple medical and technical personnel and can be time-consuming and monotonous. The VMAT technique is capable of forming multiple targets within the irradiation field, that is, multiple lesions can be irradiated and treated within a single irradiation area; therefore, it is possible to use the VMAT technique with a linear accelerator to simultaneously irradiate multiple mice to construct a mouse model for precision radiotherapy.

The TLD (LIF: Mg, Cu, P) chosen for this experiment is susceptible to dose decay and a super linear energy response in high-dose measurements and cannot be used repeatedly; other alternatives such as the (LIF: Mg, Ti) TLD and other material radiometers are more advantageous in the field of high-dose measurements [33]. However, TLD (LIF: Mg, Cu, P) is of interest in the field of low-dose measurement owing to its high sensitivity and good tissue equivalence. Lonski et al. concluded that the sensitivity of TLD (LIF: Mg, Cu, P) is sufficient for measuring out-of-field doses 50 cm from the isocenter [34]. Perera et al. suggested that the TLD skin dose measurement may help modify the geometry of brachytherapy implants and reduce late skin toxicity [35]. As the radiation dose received by patients in radiation therapy cannot be directly measured in the body, TLD (LIF: Mg, Cu, P) can measure the dose to normal tissues and endangered organs at low doses in oncological radiation therapy. This may be advantageous for determining the skin dose in breast cancer patients undergoing linear accelerator radiotherapy, crystal exposure in nasopharyngeal cancer patients, and oral mucosa radiation exposure [22]. In summary, this experiment confirmed that TLDs of different sizes have good linear responses under a linear accelerator and can be applied in clinical dosimetry. The physical experimental data provide a physical dose reference range for the construction of an accurate biological model of RILD. Data from the biological experiments demonstrated the pathological symptoms of RILD at the irradiated liver sites; the differences in the location of the radiated liver were not significant, which confirmed the reliability of the physical experimental data. Thus, the VMAT technique can be used to construct a precise model of RILD in mice under a linear accelerator.

5 Conclusion

The deviation in the measured and prescribed doses of TLD in the mouse liver ranged from − 1.5 to 6%; construction of an accurate model of RILD using the VMAT technique under a linear accelerator is feasible.

Acknowledgements In this experiment, we would like to thank Prof. Dong-Lai Lv for his suggestions on the article and structure, and Sha-Sha Yang for her contribution onto the pathological results in mice.

Author contributions All authors contributed to the study conception and design. Material preparation, data collection and analysis were performed by Hui-Hui Xiao, Ling-Ling Liu, Wen-Yi Li and Zong-Tao Hu. The first draft of the manuscript was written by Hui-Hui Xiao, and all authors commented on previous versions of the manuscript. All authors read and approved the final manuscript.

Data availability The data that support the findings of this study are openly available in Science Data Bank at https://doi.org/10.57760/sciencedb.07260 and https://cstr.cn/31253.11.sciencedb.07260.

Declaration

Ethical approval This study and included experimental procedures were approved by The Medical Ethics Committee of Hefei Cancer Hospital, Chinese Academy of Sciences (approval no. DW-LL2022-001). All animal housing and experiments were conducted in strict accordance with the institutional guidelines for care and use of laboratory animals. Written informed consent was obtained from all the participants prior to the enrollment of this study.

References

1. G.W. Chen, Q. Zhao, B.Y. Yuan et al., ALKBH5-modified HMGB1-STING activation contributes to radiation induced liver disease via innate immune response. Int. J. Radiat. Oncol. Biol. Phys. **111**(2), 491–501 (2021). https://doi.org/10.1016/j.ijrobp.2021.05.115
2. M. Spalding, A. Walsh, H. Clarke et al., Evaluation of a new hybrid VMAT-IMRT multi-criteria optimization plan generation algorithm. Med. Dosim. **45**(1), 41–45 (2020). https://doi.org/10.1016/j.meddos.2019.05.002
3. Z.G. Ahmadi, E.K. Mohammad, A.M. Ali, Dosimetry calculations of involved and noninvolved organs in proton therapy of liver cancer: a simulation study. Nucl. Sci. Tech. **30**, 173 (2019). https://doi.org/10.1007/s41365-019-0698-8
4. T. Li, Y. Cao, B. Li et al., The biological effects of radiation-induced liver damage and its natural protective medicine. Prog.

Biophys. Mol. Biol. **167**, 87–95 (2021). https://doi.org/10.1016/j.pbiomolbio.2021.06.012
5. C.M.C. Ma, I.J. Chetty, J. Deng et al., Beam modeling and beam model commissioning for Monte Carlo dose calculation-based radiation therapy treatment planning: report of AAPM Task Group 157. Med. Phys. **47**(1), e1–e18 (2020). https://doi.org/10.1002/mp.13898
6. A.G. Livingstone, S.B. Crowe, S. Sylvander et al., Clinical implementation of a Monte Carlo based independent TPS dose checking system. Phys. Eng. Sci. Med. **43**(3), 1113–1123 (2020). https://doi.org/10.1007/s13246-020-00907-x
7. P.F. Shen, X.D. Huo, Z. Shao et al., Mesh-free semi-quantitative variance underestimation elimination method in Monte Caro algorithm. Nucl. Sci. Tech. **34**, 14 (2023). https://doi.org/10.1007/s41365-022-01156-1
8. L.A. DeWerd, K. Kunugi, Accurate dosimetry for radiobiology. Int. J. Radiat. Oncol. Biol. Phys. **111**(5), e75–e81 (2021). https://doi.org/10.1016/j.ijrobp.2021.09.002
9. C. Jin, H. Liu, W. Li et al., Biological effects of human lung cells MRC-5 in CBCT positioning for image-guided radiotherapy. Nucl. Sci. Tech. **28**, 72 (2017). https://doi.org/10.1007/s41365-017-0225-8
10. H.J. Li, S.X. Jiao, Z.B. Chen et al., Study of beam model of medical linear accelerator based on virtual single point source. Nucl. Tech. **44**(04), 040202 (2021). https://doi.org/10.11889/j.0253-3219.2021.hjs.44.040202 (**in Chinese**)
11. Q. Lyu, D. O'Connor, D. Ruan et al., VMAT optimization with dynamic collimator rotation. Med. Phys. **45**(6), 2399–2410 (2018). https://doi.org/10.1002/mp.12915
12. P. Alvarez, S.F. Kry, F. Stingo et al., TLD and OSLD dosimetry systems for remote audits of radiotherapy external beam calibration. Radiat. Meas. **106**, 412–415 (2017). https://doi.org/10.1016/j.radmeas.2017.01.005
13. T. Kato, T. Sagara, S. Komori et al., Dosimetric properties of a newly developed thermoluminescent sheet-type dosimeter for clinical proton beams. J. Appl. Clin. Med. Phys. **22**(4), 158–165 (2021). https://doi.org/10.1002/acm2.13222
14. P. Kuess, E. Bozsaky, J. Hopfgartner et al., Dosimetric challenges of small animal irradiation with a commercial X-ray unit. Z. Med. Phys. **24**(4), 363–372 (2014). https://doi.org/10.1016/j.zemedi.2014.08.005
15. I.V. Karagounis, I.M. Abatzoglou, M.I. Koukourakis, Technical Note: Partial body irradiation of mice using a customized PMMA apparatus and a clinical 3D planning/LINAC radiotherapy system**.** Med. Phys. **43**(5), 2200–2206 (2016). https://doi.org/10.1118/1.4945274
16. V.M. López-Guadalupe, A. Rodríguez-Laguna, M.A. Poitevin-Chacón et al., Out-of-field mean photon energy and dose from 6 MV and 6 MV FFF beams measured with TLD-300 and TLD-100 dosimeters. Med. Phys. **48**(11), 6567–6577 (2021). https://doi.org/10.1002/mp.15233
17. S.M. Ghoneam, K.R. Mahmoud, H.M. Diab et al., Studying the dose level for different X-ray energy conventional radiography by TLD-100. Appl. Radiat. Isot. **181**, 110066 (2022). https://doi.org/10.1016/j.apradiso.2021.110066
18. L. Deng, N. Zhou, S.G. Qu et al., MCNP simulation of X-ray beam for a 15 MV medical linear accelerator. Nucl. Tech. **44**(11), 110202 (2021). https://doi.org/10.11889/j.0253-3219.2021.hjs.44.110202 (in Chinese)
19. R. De Roover, W. Crijns, K. Poels et al., Validation and IMRT/VMAT delivery quality of a preconfigured fast-rotating O-ring linac system. Med. Phys. **46**(1), 328–339 (2019). https://doi.org/10.1002/mp.13282
20. M.S.A. Fadzil, N.M. Noor, N. Tamchek et al., A cross-validation study of Ge-doped silica optical fibres and TLD-100 systems for high energy photon dosimetry audit under non-reference conditions. Radiat. Phys. Chem. **200**, 110232 (2022). https://doi.org/10.1016/j.radphyschem.2022.110232
21. Y.S. Horowitz, L. Oster, I. Eliyahu, The saga of the thermoluminescence (TL) mechanisms and dosimetric characteristics of LiF:Mg, Ti (TLD-100). J. Lumin. **214**, 116527 (2019). https://doi.org/10.1016/j.jlumin.2019.116527
22. Y.C. Chen, H.C. Lin, W.H. Lai et al., Evaluating dose distributions of normal organs for patients undergoing VMAT therapy of nasopharyngeal carcinoma using Rando phantom and TLD-100H. Technol. Health Care. **30**(S1), 329–336 (2022). https://doi.org/10.3233/THC-THC228031
23. H. Acun-Bucht, E. Tuncay, E. Darendeliler et al., Absolute dose verification of static intensity modulated radiation therapy (IMRT) with ion chambers of various volumes and TLD detectors. Rep. Pract. Oncol. Radiother. **23**(4), 242–250 (2018). https://doi.org/10.1016/j.rpor.2018.04.001
24. A. Ketabi, S. Karbasi, R. Faghihi et al., A phantom-based experimental and Monte Carlo study of the suitability of in-vivo diodes and TLD for entrance in-vivo dosimetry in small-to-medium sized 6 MV photon fields. Radiat. Phys. Chem. **201**, 110411 (2022). https://doi.org/10.1016/j.radphyschem.2022.110411
25. I.J. Das, P. Francescon, J.M. Moran et al., Report of AAPM task group 155: Megavoltage photon beam dosimetry in small fields and non-equilibrium conditions. Med. Phys. **48**(10), e886–e921 (2021). https://doi.org/10.1002/mp.15030
26. B. Jones, Clinical radiobiology of proton therapy: modeling of RBE. Acta Oncol. **56**(11), 1374–1378 (2017). https://doi.org/10.1080/0284186X.2017.1343496
27. A.L. Palmer, S.M. Jafari, I. Mone et al., Evaluation and clinical implementation of in vivo dosimetry for kV radiotherapy using radiochromic film and micro-silica bead thermoluminescent detectors. Phys. Med. **42**, 47–54 (2017). https://doi.org/10.1016/j.ejmp.2017.08.009
28. X.M. Wan, X.J. Pu, Z.Q. Ren et al., Discussion of 90° stopband in low-energy superconducting linear accelerators. Nucl. Sci. Tech. **33**, 121 (2022). https://doi.org/10.1007/s41365-022-01104-z
29. B. Jones, S.J. McMahon, K.M. Prise, The radiobiology of proton therapy: challenges and opportunities around relative biological effectiveness. Clin. Oncol. (R Coll Radiol) **30**(5), 285–292 (2018). https://doi.org/10.1016/j.clon.2018.01.010
30. R. Singh, H. Al-Hallaq, C.A. Pelizzari et al., Dosimetric quality endpoints for low-dose-rate prostate brachytherapy using biological effective dose (BED) vs. conventional dose. Med. Dosim. **28**(4), 255–259 (2003). https://doi.org/10.1016/j.meddos.2003.04.001
31. S. Du, G. Chen, B. Yuan et al., DNA sensing and associated type 1 interferon signaling contributes to progression of radiation-induced liver injury. Cell Mol. Immunol. **18**(7), 1718–1728 (2021). https://doi.org/10.1038/s41423-020-0395-x
32. F. Dong, X. Weng, X. Deng et al., Clinical utility of a new immobilization method in image-guided intensity-modulated radiotherapy for breast cancer patients after radical mastectomy. J. Xray Sci. Technol. **30**(4), 641–655 (2022). https://doi.org/10.3233/XST-221127
33. M. Alizadeh, M. Mohseni, B. Farhood et al., Thermoluminescent Characteristics of GR-200, TLD-700H and TLD-100 for low dose measurement: linearity, repeatability, dose rate and photon energy dependence. J. Biomed. Phys. Eng. **12**(2), 111–116 (2022). https://doi.org/10.31661/jbpe.v0i0.1247
34. P. Lonski, S. Keehan, S. Siva et al., Out-of-field in vivo dosimetry using TLD in SABR for primary kidney cancer involving mixed photon fields. Phys. Med. **37**, 9–15 (2017). https://doi.org/10.1016/j.ejmp.2017.03.022
35. F. Perera, F. Chisela, L. Stitt et al., TLD skin dose measurements and acute and late effects after lumpectomy and high-dose-rate brachytherapy only for early breast cancer. Int. J. Radiat. Oncol. Biol. Phys. **62**(5), 1283–1290 (2005). https://doi.org/10.1016/j.ijrobp.2005.01.007